MET O 19 BRANCH MEMORANDUM No. 46

TROPOSPHERIC RETRIEVALS FROM A SATELLITE PASSIVE MICROWAVE SPECTROMETER.

by

D. Offiler Met. O. 19

OCTOBER 1978

Met O 19
(High Atmosphere Branch)
Meteorological Office
London Road
BRACKNELL
Berks RG12 2SZ

FH33

LBN

BM No. 46

TROPOSPHERIC RETRIEVALS FROM A SATELLITE PASSIVE MICROWAVE SPECTROMETER

by D Offiler, October 1978.

Summary

This note describes the method and some results of retrieving tropospheric quantities (temperature, thickness, total water vapour and liquid water) from the Nimbus 6 Scanning Microwave Spectrometer (SCAMS) brightness temperatures. Retrieval standard differences of 2.2K in 500 mb temperature and 2.6 Dm in 1000-500 mb thickness have been obtained when compared with an independent set of colocated radiosonde ascents.

1. Introduction

Several authors (such as Grody (1976), Grody & Pellegrino (1977), Kunzi et al (1976), Rosenkranz et al (1976, 1978), Staelin et al (1976), Waters et al, (1975) and Wilcox et al(1976)) have previously deduced various meteorological data from passive microwave radiometers. This note describes the methods used in Met O 19 to retrieve standard pressure level temperatures and thicknesses, together with total water vapour and liquid water contents from the Scanning Microwave Spectrometer (SCAMS) instrument flown on Nimbus 6. The bases of these methods are from the above references, in particular from Grody & Pellegrino. Two periods were chosen for study: August 1975 and February 1976, with a total of twenty-two satellite passes over seven separate days.

Although at present, passive microwave instruments have only a few temperature sounding channels and poor vertical and horizontal resolution compared with infrared spectrometers, their sounding measurements are not greatly affected by even thick clouds or light rain (Staelin et al 1975b). This enables much more complete coverage than with infrared instruments, though to a lesser degree of accuracy when both types of retrieval are available (ie in cloud-free areas).

2. Microwave Radiometry

At microwave frequencies (corresponding to a wavelength range of 0.3 to 30 cm in common usage), the Planck function is very well represented by the Rayleigh-Jeans approximation, where the radiance is linearly dependent on the emitting temperature of the object. Hence the term 'brightness temperature' is used in

place of 'radiance'. The brightness temperature (BT) measured by a satellite-borne instrument at frequency ν and zenith angle θ is $T_B(\nu, \theta)$ and is related to the vertical profile of atmospheric temperature, T(h), by the radiative transfer equation:

$$T_B(\nu,\theta) = \tau_\nu(0)^{\sec\theta} \cdot \varepsilon_s \cdot T_s + \int_0^H T(h) \cdot W(\nu,\theta,h)\, dh \qquad \ldots\ldots (1)$$

where $$W(\nu,\theta,h) = \left\{1 + \left[1-\varepsilon_s(\nu,\theta)\right]\left(\frac{\tau_\nu(0)}{\tau_\nu(h)}\right)^{2\sec\theta}\right\} \cdot \frac{\partial \tau_\nu(h)}{\partial h}^{\sec\theta} \qquad \ldots\ldots (2)$$

and $$\tau_\nu(h) = \exp\left(-\int_h^H (\alpha_o(\nu,z) + \alpha_v(\nu,z) + \alpha_c(\nu,z) + \alpha_R(\nu,z))\, dz\right) \qquad \ldots\ldots (3)$$

is the atmospheric transmittance at frequency ν from height h to the satellite height H. ($\tau_\nu(0)$ is the total transmittance from the surface to H), and $\alpha(\nu,z)$ is the attenuation coefficient at frequency ν and height z (within the slab h to H) due to oxygen, water vapour, cloud or rain. T_s is the surface temperature and ε_s the surface emissivity which depends on the polarisation vector as well as viewing angle and frequency and, for a sea surface, temperature, salinity and wind speed. For SCAMS frequencies, ε_s is about 0.4-0.6 over sea and 0.9-1.0 over land. (See Appendix I for further detail of emissivity variation). None of the microwave retrieval references state whether surface emissivity variations were more accurately represented: only the above ranges or "about 0.5 over sea" are quoted. This study explicitly calculated ε_s for each individual case.

Equation (1) shows the separate contributions to the BT of the surface (first term) and atmosphere. The small contributions from the 2.7K space BT, partially reflected from the surface and attenuated both ways (at most 0.5K), and non-specular emission from the sun are neglected. The quantity $W(\nu, \theta, h)$ is the temperature weighting function, which indicates the relative contribution to the BT from each level for a given frequency and zenith angle, and is essentially the derivative of the transmittance function with height. The second term in the braces of equation (2) allows for the downward atmospheric emission reflected from the surface and attenuated each way, and is particularly important over the sea because of its relatively high reflectivity (~ 0.5).

3. The SCAMS Instrument

Atmospheric temperature and water content are the principal parameters derivable from microwave radiometric measurements made in the 60 GHz oxygen band and 22 GHz water vapour line respectively.

The SCAMS instrument consists of five independent radiometers detecting thermal microwave emission at 52.85, 53.85 and 55.45 GHz (oxygen), 22.23 and 31.65 GHz (water vapour). The radiometer mechanism scans $\pm$ 43.2° either side of nadir in increments of 7.2°, allowing a swath of thirteen spots with zenith angles of 0, 8.4, 16.9, 25.5, 34.4, 43.4 and 53.2°. The antennae have 7.5° beamwidths (3dB) resulting in spots of about 145 x 145 km at nadir to 360 x 220 km at 53°. Two further steps allow calibration with cold space (about 2.7K) and a temperature monitored target. The scan pattern is shown in Figure 1.

The SCAMS polarisation vector is horizontal (parallel to the sub-satellite track) at nadir and rotates to about 40% horizontal, 60% vertical at the extreme scan angles. Further details of the SCAMS instrument may be found in the Nimbus 6 Users Guide, Staelin et al (1975a).

The weighting functions for the three oxygen channels only vary a little with temperature and are dependent on composition (water vapour, cloud and rain) and zenith viewing angle. Figure 2 shows the weighting functions at nadir and 53°, and the effects of the different emissivity of sea and land surfaces, for clear skies. The two lower frequency channels are on the extreme wings of the oxygen band, and are primarily affected by water vapour and liquid water absorption. Channel 1 (22 GHz) is at the peak of the water vapour absorption line, and channel 2 (31.65 GHz) is between the water vapour and oxygen absorption areas. Figure 3 is a plot of calculated BT with frequency (nadir view) with different atmospheres. Curve (a) shows the surface emission, with no atmosphere, of a calm sea at 288K; curve (b) due to (a) plus oxygen absorption only for a midlatitude summer standard atmosphere temperature profile (McClatchey et al 1972); curve (c) has an added 2.2 g cm^{-2} water vapour distributed as 10 exp (-h/2.2) g/kg and (d) a layer of cloud with 0.2 mm of liquid water. Curve (e) shows the effect of 1 mm/hr rainfall added to (d).

4. The Retrieval Method

Equation (1) may be statistically inverted to give a linear relationship between atmospheric temperature profile and a set of BTs:

$$T(h) = a_0(h,\theta) + \sum_{n=1}^{5} a_1(\nu_n, h, \theta).T_B(\nu_n, \theta) \quad \ldots\ldots (4)$$

In practice, it is more convenient to work at standard pressure levels, and h is replaced by p. Equation (4) is a linear multiple regression solution to equation (1), with regression coefficients $a(\nu_n, p, \theta)$. This procedure will be referred to as Method A. Method B involves first reducing the BTs, at scan angle θ, to their equivalent nadir value by simple regression,

$$\text{ie} \quad T_B(\nu_n) = b_0(\nu_n, \theta) + b_1(\nu_n, \theta).T_B(\nu_n, \theta) \quad , n = 1,5 \quad \ldots\ldots (5)$$

Only one common set of b's are required for any retrieval, necessitating only a single set of regression coefficients $a(\nu_n, p)$, which are independent of viewing angle:

$$T(p) = a_0(p) + \sum_{n=1}^{5} a_1(\nu_n, p).T_B(\nu_n) \quad \ldots\ldots (6)$$

This greatly reduces the total number of coefficients needed if more than about three separate quantities are to be retrieved. (21 quantities were retrieved in this study). None of the references dealing with actual SCAMS retrievals (the Nimbus-E Microwave Spectrometer (NEMS) was a non-scanning instrument) state whether the scan angle was taken into account or not. Grody & Pellegrino make use of scan angle in deriving regression coefficients and presumably use the Method A in their case studies.

Although the spread of each weighting function in Figure 2 indicates the vertical resolution of any one measurement, the linear combination of equation (4) or (6) improves the effective resolution, and increased accuracy is obtainable with the statistical information contained in the coefficients.

Using a model based on equations (1), (2) and (3), (the details of which are explained in Appendix II), simulated BTs at the five SCAMS channel frequencies and at seven scan angles were obtained from each of four hundred midlatitude radiosonde profiles. These had cloud layers artificially introduced - see Appendix III. Model BTs were verified with a set of twenty-one ship radiosondes (stations, L, M and R) colocated with actual SCAMS measurements during the periods previously mentioned.

The regression coefficients for pressure level temperatures and (1000-p)mb thicknesses at the standard levels of 1000, 850, 700, 500, 400, 300, 250, 200, 150 and 100 mb, and those for total water vapour and liquid water were computed using the simulated BTs and the sample ascents. Through equation (1) these coefficients contain statistics on local surface emissivity changes, but the large difference between land and sea necessitates a separate set of coefficients for these two cases. Water vapour and liquid water retrievals can only be done over sea surfaces, since over land, the surface BT is similar to that of the atmospheric water, and hence it shows up neither in emission nor absorption.

5. Results

(N.B. The term 'error' (as in 'standard error') is used to denote the algebraic difference between a retrieved value and the true atmospheric condition. The term 'difference' (as in 'standard difference') refers to the algebraic difference between a retrieved value and the measured one - which has an 'error' of its own. The dependent sample of profiles is assumed to represent true atmospheric values).

5.1 Temperature and thickness retrievals

Figure 4 (i)-(ii) shows the sample standard deviations of temperature and thickness and the standard errors of the estimate (the rms residual errors of the retrieval, about the mean, from the dependent sample) for the set of 400 profiles used. The standard error is a measure of the theoretical limit of the SCAMS accuracy since any errors or biases in the model will not appear in a regression analysis using model-derived BTs. The difference between the two lines at any level indicates the extent of the information content in the BT 'measurements'. The large errors in temperature at the surface for the sea case are due to the large emissivity variations because of (in the real world) surface roughness, foam, salinity variations etc., and the errors at about 200 mb are due to the weighting functions not resolving the tropopause. In the following results, it was found that Method B (reducing the BTs to their nadir equivalents) gave slightly better results, particularly below 300 mb, than Method A. Since Method B requires far fewer coefficients, all the results presented, derived from actual SCAMS measurements, used this method.

Figure 5 (i)-(xii) shows some retrieved temperature profiles (solid line) compared with colocated radiosonde ascents (dashed line). The error in interpolating the individual BTs to the ships' positions may be $\pm$ 0.5K and the satellite passes are $\pm$ 2 hours of the ascents. The regression coefficients used only apply to discrete zenith angles. It is estimated that there may be an error of up to 2K in any individual level temperature retrieval for these reasons. It is seen that in most cases the retrieved temperatures in the troposphere are within 2K of the radiosonde value with which it is compared. There is a mean difference of about 1K in the troposphere (above the surface) and about -2.5K above 200 mb, with standard differences roughly 2-3K and 3-5K respectively. The thickness retrievals by direct regression are marginally worse than those obtained indirectly from the retrieved level temperatures, but the former method is easier to apply. A standard difference of 2.6 Dm in 500 mb thickness was found. The small sample size (N = 21) does not allow any significant correlations in differences to be made with surface wind speed, cloud, scan angle etc. (The other nine comparisons not shown were no better or worse than those presented).

Figure 6 (i)-(ii) shows the colocated sonde standard deviations and their retrieval standard differences in a similar way to Figure 4. In the thickness retrievals (Figure 6 (ii)), curve (a) is for a computation of thickness from the retrieved temperature profile and curve (b) for direct retrieval. The mean differences and standard deviations are also presented in Table 1.

Since the most common and easily obtainable analysed charts are those for 1000-500 mb thickness, effort has been concentrated on retrieving this quantity from the SCAMS BTs. In all, 22 Nimbus 6 passes in the area bounded by 15 and 65°N, 80°W and 30°E on the 20, 27 August 1975 and 1, 2, 9, 14 and 19 February 1976 were obtained. Figure 7 (i)-(vii) shows the patterns of SCAMS retrievals (solid lines) compared with the subjectively analysed CFO charts. At least two adjacent passes have been used in each case, and all are within three hours of the chart time. The high density of retrieval points allows easy objective analysis of the SCAMS lines. The only subjective

fitting is at the edges of consecutive swaths where the contours do not join exactly. All the SCAMS spots are usable: the density of retrieved values is indicated in Figure 8, a typical SCAMS swath. (The single pass retrievals over a limited area, and not presented here, showed similar accuracies). It can be seen that the major trough-ridge features and their thermal gradients are well retrieved, both over land and sea. Over all the cases, there does not appear to be any great bias in thickness values, except south of about 30°N, where there are few conventional observations and extreme land surface temperatures. Here, the retrievals average about 6-9 Dm high. North of about 65°N, the retrievals are about 3-6 Dm low, in the February cases possibly because the surface is of ice. (Strictly, the retrieval coefficients only apply to the region 30-60°N, the coverage of the original sample of midlatitude radiosonde ascents).

In all the cases, there was extensive cloud cover; over large areas, it would be impossible to obtain a meaningful retrieval from an IR sounding, even with cloud clearing techniques. Clouds do not appear to have affected the SCAMS patterns when compared with the closest nephanalyses.

5.2 Water Vapour and Liquid Water Retrievals

The inclusion of two channels which respond to water vapour and liquid water amounts permit 'corrections' for the small effects of vapour and cloud on the oxygen channels in the regression equations. However, they are primarily intended to enable estimates to be made of these quantities directly. (Grody, 1976, Staelin et al, 1976). Comparison of the water vapour content derived from the colocated ascents and the SCAMS derived values (N = 21) show a mean difference of 0.7 mm and standard difference of 3.8 mm. The standard error for the dependent sample of 400 was 2.0 mm. (Typical values of water vapour are 5-30 mm).

Liquid water retrievals are difficult to verify quantitatively since no routine measurements are made, and cannot be estimated from a radiosonde ascent, except very crudely. A rough estimate can be made by minimising the errors between SCAMS measured BTs and the simulated values from the colocated

sondes by varying the liquid water content in the model. This method gave a mean difference of 4.2 mg cm^{-2} and standard difference of 6.3 mg cm^{-2} with typical values of 0-50 mg cm^{-2} for non-precipitating clouds. Comparison of the SCAMS liquid water fields were made with the nephanalyses closest in time to the Nimbus 6 passes. These showed good correlation of higher values (> 15 mg cm^{-2}) of liquid water with areas of 'significant' cloud, the highest retrieved values being about 60 mg cm^{-2} over the open sea. It should be remembered that the retrieved values represent averages over quite large areas, at least 20000 km^2; large liquid water contents in cumuliform clouds will tend to be underestimated due to their small horizontal fractional cover. Small features evident on the nephanalyses are not resolved by the SCAMS instrument, but synoptic scale features are resolved and an estimate of the relative liquid water content, if not accurate absolute amounts, can be deduced.

6. Conclusions

Retrievals of tropospheric temperatures, thicknesses and atmospheric water have been made using microwave sounding data. Even though at present, the instruments have only a few channels and low spatial resolution, there is good agreement with the derived quantities and conventional data. The ability of microwaves to penetrate clouds allows much higher density of coverage than with IR measurements, even when complicated cloud-clearing procedures have been applied to the latter in very cloudy areas. However, large emissivity variations over the sea, particularly due to surface wind roughness and foam generation, prevent accurate determination of surface temperature with the frequencies used. Since, for the lower two frequencies, the total transmittance is normally greater than 0.7-0.8, effects on their brightness temperatures due to emissivity changes can mask changes due to atmospheric water, making the latter retrieval an estimate rather than a 'measurement'. Again, because of the more complete coverage, such an estimate, particularly near fronts etc may be better than none at all.

Future work could include using the different attributes of IR and microwave measurements (eg HIRS and SCAMS) in conjunction rather than in competition, to enable wider coverage of more accurate retrievals.

References

Grody, N.C., 1976: Remote sensing of atmospheric water content from satellites using microwave radiometry. IEEE Trans. Antennas Propagat. AP-24, 155-162.

Grody, N.C., P.P. Pellegrino, 1977: Synoptic scale studies using the Nimbus 6 microwave spectrometer. J. Appl. Met., 16, 816-826.

Kunzi, K.F., A.G. Piaget, C.B. Ruchi, 1976: The accuracy of the terrestrial atmospheric temperature profile derived from Nimbus-5 microwave spectrometer (NEMS) data. COSPAR 8-10 June 1976, 22-29.

McClatchey, R.A., R.W. Fenn, J.E.A. Selby, F.E. Volz, J.S. Garing, 1972: Optical properties of the atmosphere. AFCRL, Envirn. Res. Papers No 411 (3rd edn), 3-7.

Rosenkranz, P.W., D.H. Staelin, R.L. Pettyjohn, 1976: Retrieval of atmospheric temperature profiles by a scanning microwave spectrometer. COSPAR 8-10 June, 1976, 20-21.

Rosenkranz, P.W., D.H. Staelin, 1978: Typhoon June (1975) viewed by a scanning microwave spectrometer. J. Geophys. Res., 83, No. C4, 1857-1868.

Staelin, D.H., A.H. Barrett, P.W. Rosenkranz, F.T. Barath, E.J. Johnson, J.W. Waters, A. Wouters, W.B. Lenoir, 1975a: The scanning microwave spectrometer (SCAMS) experiment. Nimbus 6 User's Guide, Goddard Space Flight Centre, 59-86.

Staelin, D.H., A.L. Cassel, K.F. Funzi, R.L. Pettyjohn, R.K.L. Poon, P.W. Rosenkranz, J.W. Waters, 1975b: Microwave Atmospheric Temperature sounding: effects of clouds on the Nimbus 5 data. J. Atmos. Sci., 32, 1970-1976.

Staelin, D.H., K.F. Kunzi, R.L. Pettyjohn, R.K.L. Poon, R.W. Wilcox, J.W. Waters, 1976: Remote sensing of atmospheric water vapour and liquid water with the Nimbus 5 microwave spectrometer. J. Appl. Met., 15, 1204-1214.

Waters, J.W., K.F. Kunzi, R.L. Pettyjohn, R.K.L. Poon, D.H. Staelin, 1975: Remote sensing of atmospheric temperature profiles with the Nimbus 5 microwave spectrometer. J. Atmos. Sci. 32 1953-1969.

Wilcox, R.W., F. Sanders, 1976: Comparison of layer thickness as observed by Nimbus E microwave spectrometer and by radiosonde. J. Appl. Met., 15, 956-961.

see also:

Moyer, V., J.R. Scoggins, N-m. Chou, G.S. Wilson, 1978: Atmospheric structure deduced from routine Nimbus 6 satellite data. M.W.R., 106, 1340-1352.

Level (mb)	Radiosondes (N=21)				Retrieval (SCAMS-R/S) differences (N=21)					
	Temp (K)		Thickness (Dm)		Temp (K)		Thick (Dm) by temps		Thick (Dm) direct	
	mean	s.dev.	mean	s.dev.	mean	s.dif.	mean	s.dif.	mean	s.dif.
1000	283.5	3.9	0.0	0.0	3.5	4.3	0.0	0.0	0.0	0.0
850	271.4	5.1	131.2	2.1	0.2	3.0	1.6	1.1	0.4	1.1
700	264.7	6.0	283.5	5.3	0.0	1.8	1.6	1.7	0.3	1.8
500	249.4	6.3	536.7	11.2	- 1.0	2.2	1.0	2.6	- 0.3	2.6
400	237.8	5.9	695.8	15.1	- 0.8	1.7	0.4	3.1	- 1.1	3.2
300	223.3	6.1	889.8	19.7	0.7	3.0	0.5	3.6	- 1.1	3.8
250	216.0	6.4	1006.9	22.4	1.8	4.2	1.2	4.4	- 0.4	4.8
200	214.9	8.2	1147.1	25.5	- 0.4	3.2	2.1	5.7	0.3	6.4
150	216.3	7.2	1328.9	29.6	- 2.9	3.8	0.4	7.0	- 1.2	7.6
100	213.6	7.6	1583.9	36.3	- 2.1	4.9	- 2.7	10.3	- 4.3	11.0

Table 1. Mean and standard deviations of temperature and thicknesses for a set of colocated radiosonde ascents and SCAMS-sonde differences.

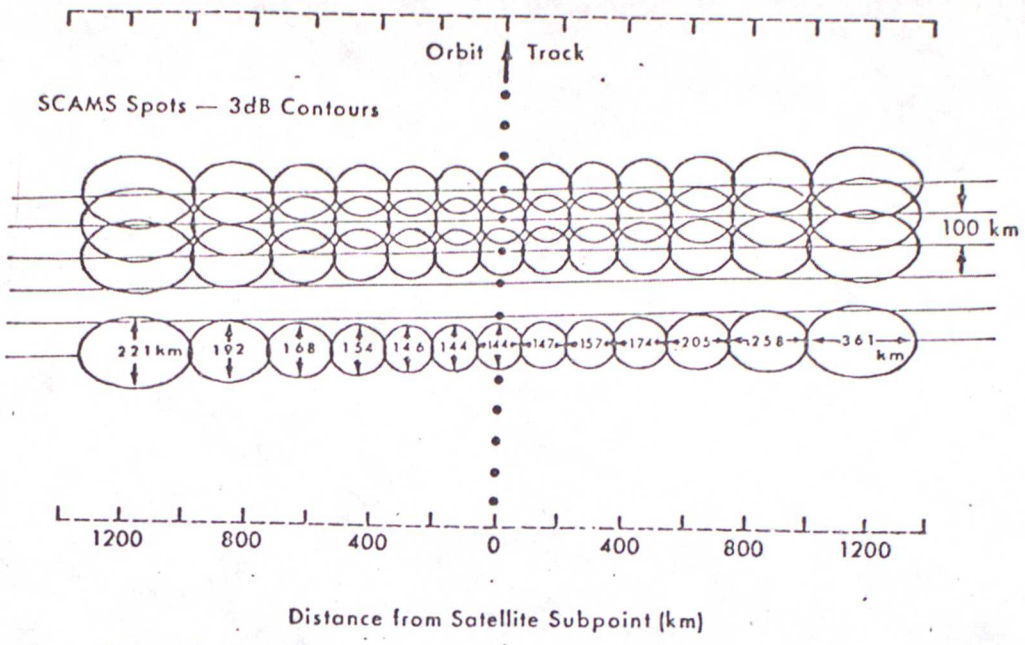

FIG. 1. Nimbus 6 SCAMS scan grid pattern and field of view projected on earth.

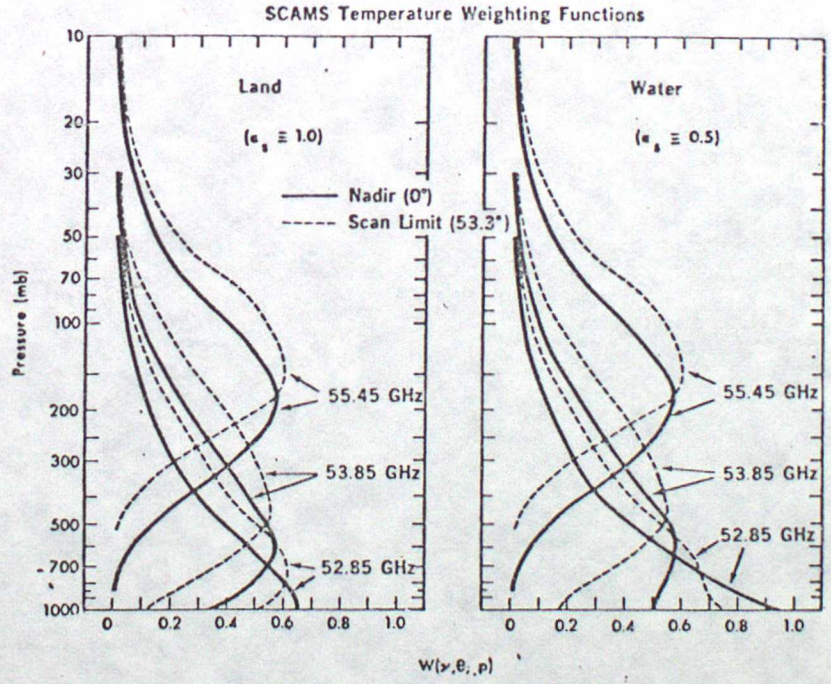

FIG. 2. SCAMS temperature weighting functions calculated for the nadir and scan limit positions for land and sea class surfaces.

Figures 1 and 2 after Grody & Pelligrino (1977).

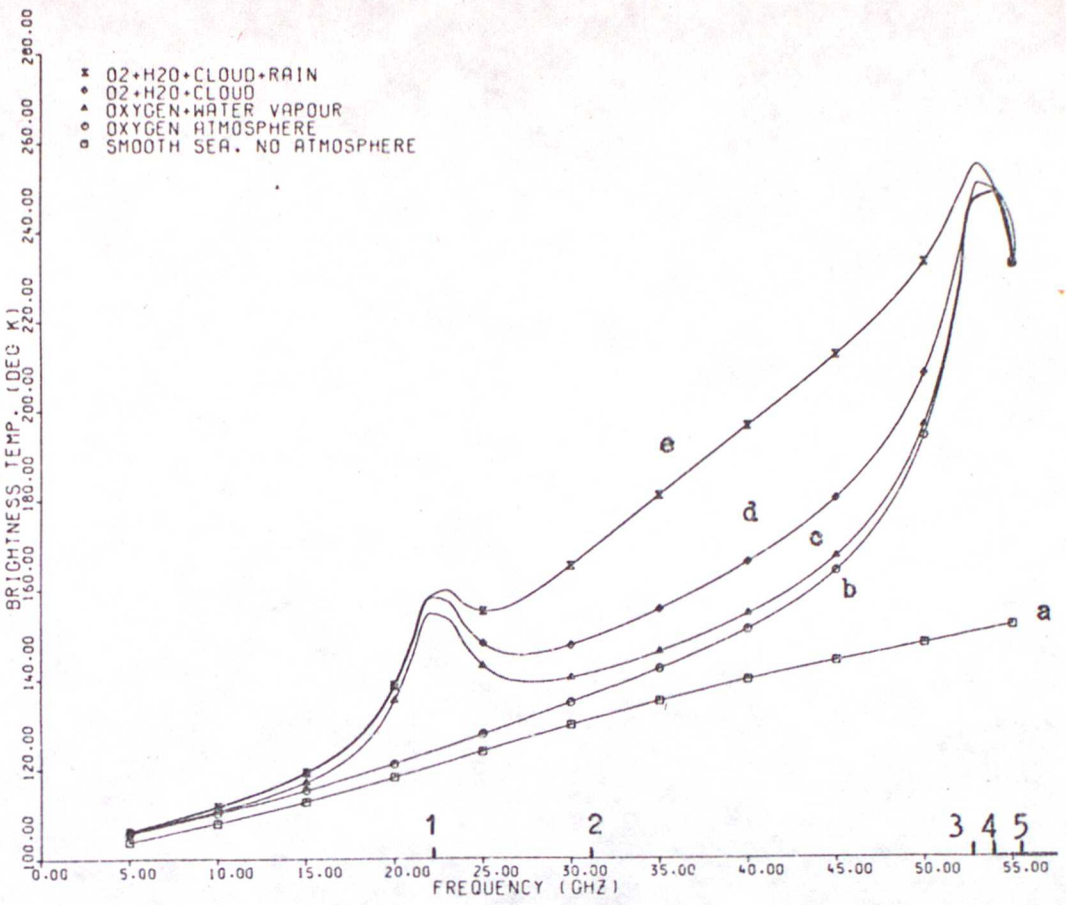

Figure 3. Variation in calculated brightness temperatures with frequency for different atmospheres.

(a) Calm sea at 288k, no atmosphere.
(b) Curve (a) plus oxygen absorption due to a midlatitude summer standard temperature profile.
(c) Curve (b) with 2.2 g/cm^2 water vapour, distributed as 10exp(-h/2.2) g/kg. (h in km)
(d) Curve (c) with a cloud layer of 0.2 mm liquid water.
(e) Curve (d) with 1 mm/hr rainfall.

The figures above the abscissa refer to the SCAMS channel numbers.

Figure 4. Sonde sample standard deviations and retieval standard errors of (i) temperature and (ii) thickness.

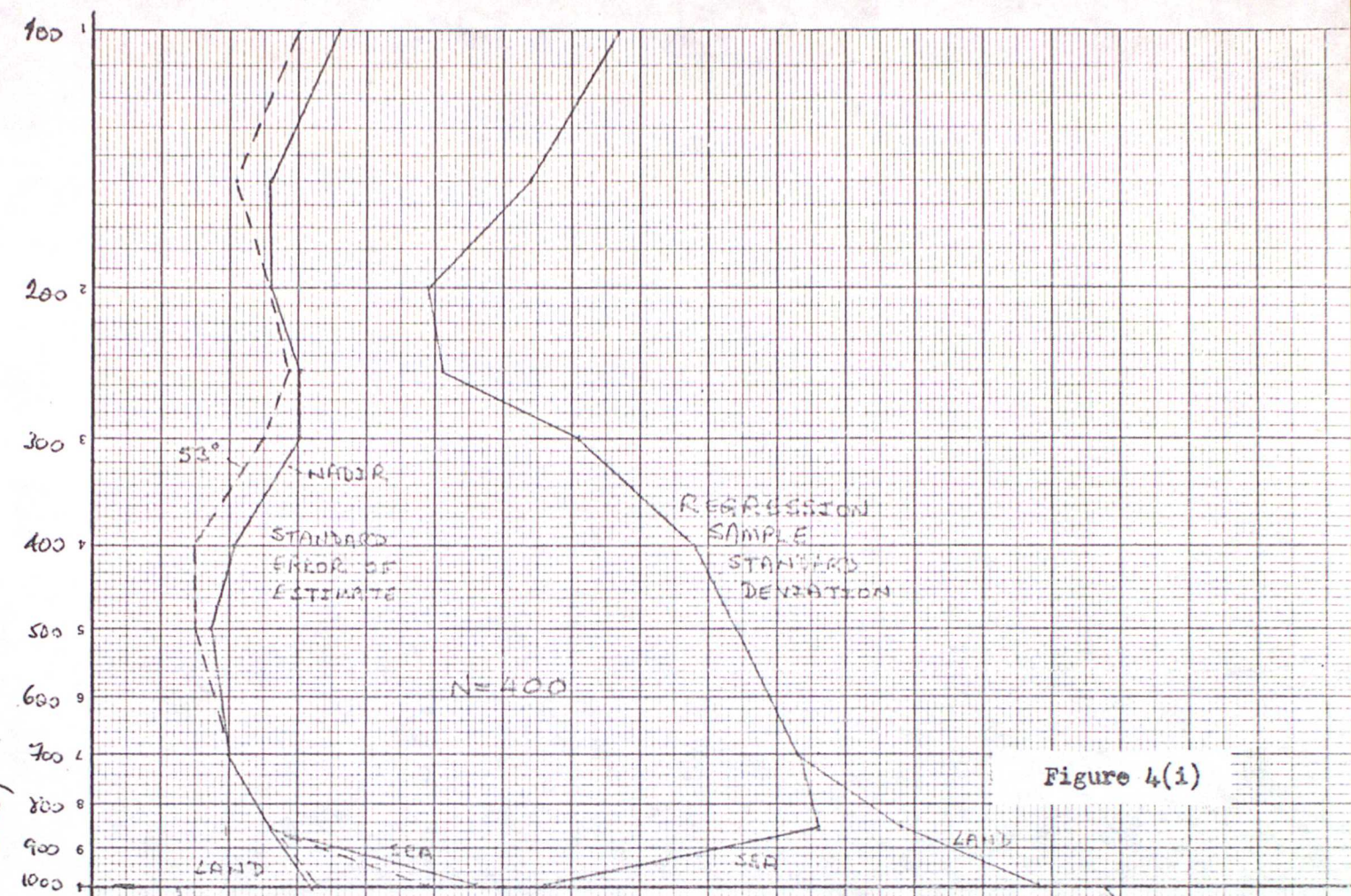

Figure 4(i)

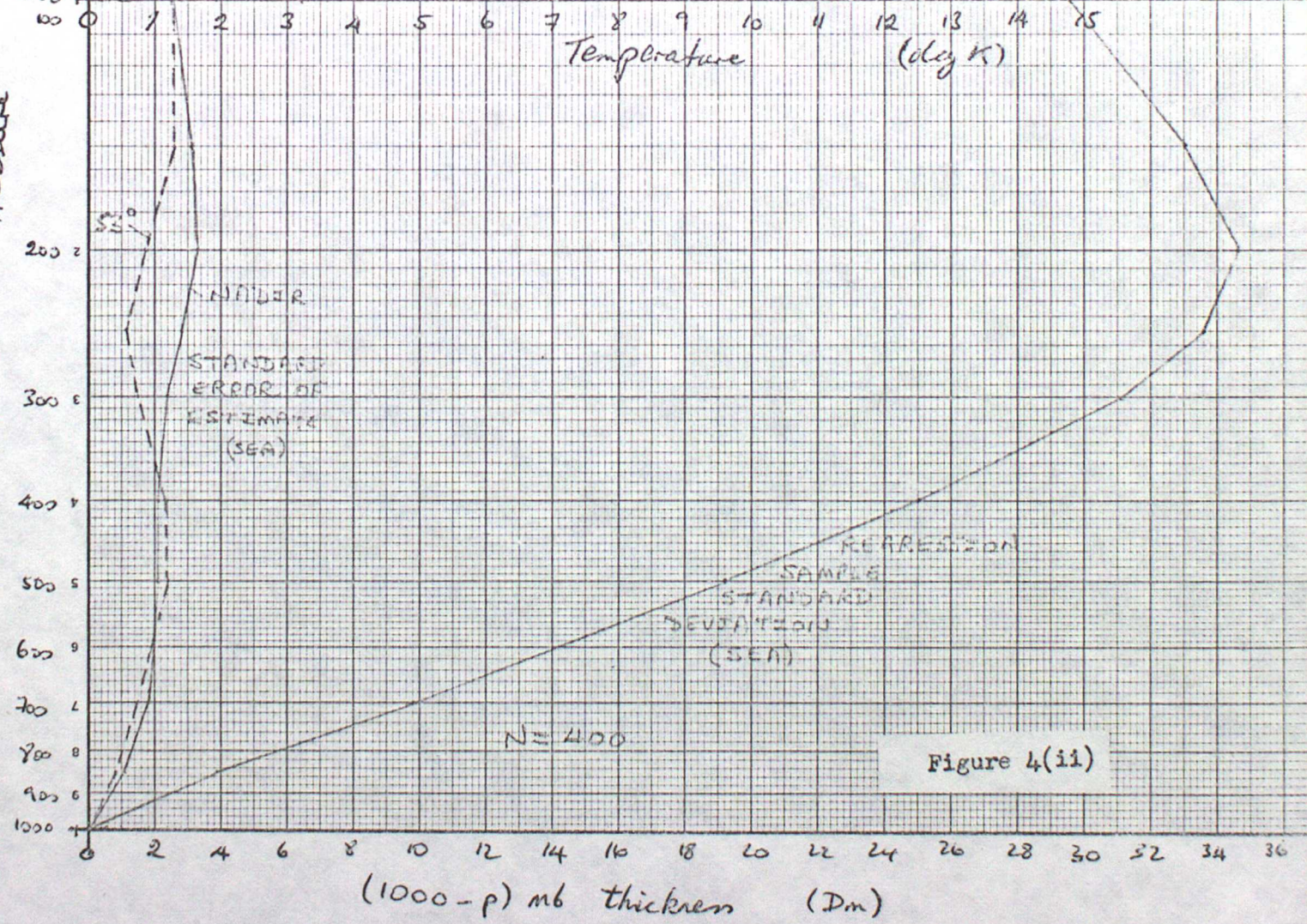

Figure 4(ii)

Figure 5. Temperature profiles from SCAMS retrievals (solid lines) and colocated radiosondes (dashed lines) for:

(i)	Ship	L			
(ii)		M	12Z	20	August 1975
(iii)		R			
(iv)		L	12Z	27	
(v)		R	00Z	1	
(vi)		L	00Z	2	
(vii)		L	12Z	2	
(viii)		M	12Z	2	February 1976
(ix)		M	12Z	9	
(x)		R	12Z	9	
(xi)		L	12Z	19	
(xii)		M	12Z	19	

The figures in the bottom left corner of each plot refer to the time of the satellite overpass, zenith angle, cloud cover and height, and surface wind speed.

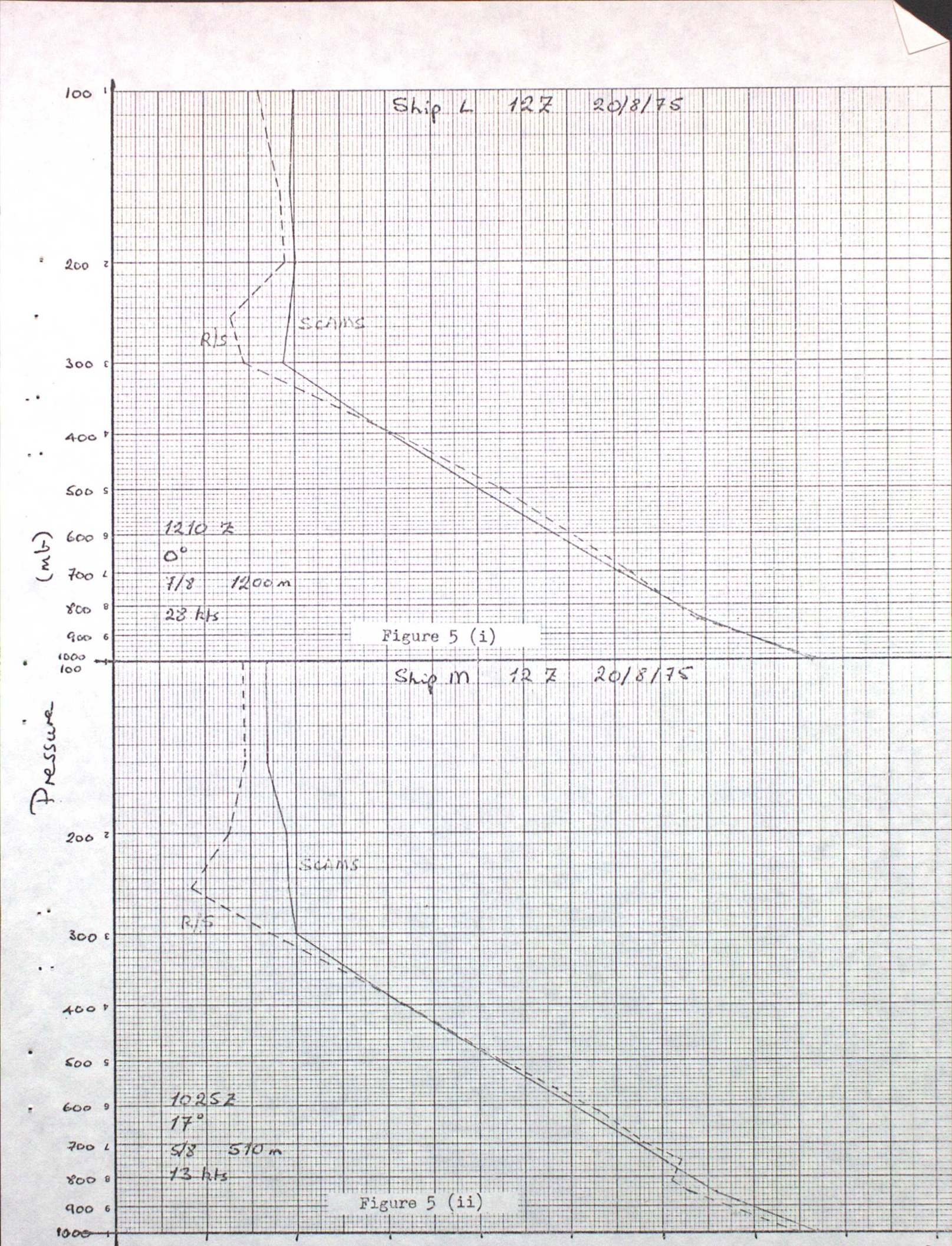
Ship L 12Z 20/8/75
RIS
SCAMS
1210 Z
0°
7/8 1200m
28 kts
Figure 5 (i)
Ship M 12 Z 20/8/75
SCAMS
RIS
1025Z
17°
5/8 510 m
13 kts
Figure 5 (ii)
Pressure (mb)
Temperature (K)
100
200
300
400
500
600
700
800
900
1000
210
220
230
240
250
260
270
280
290

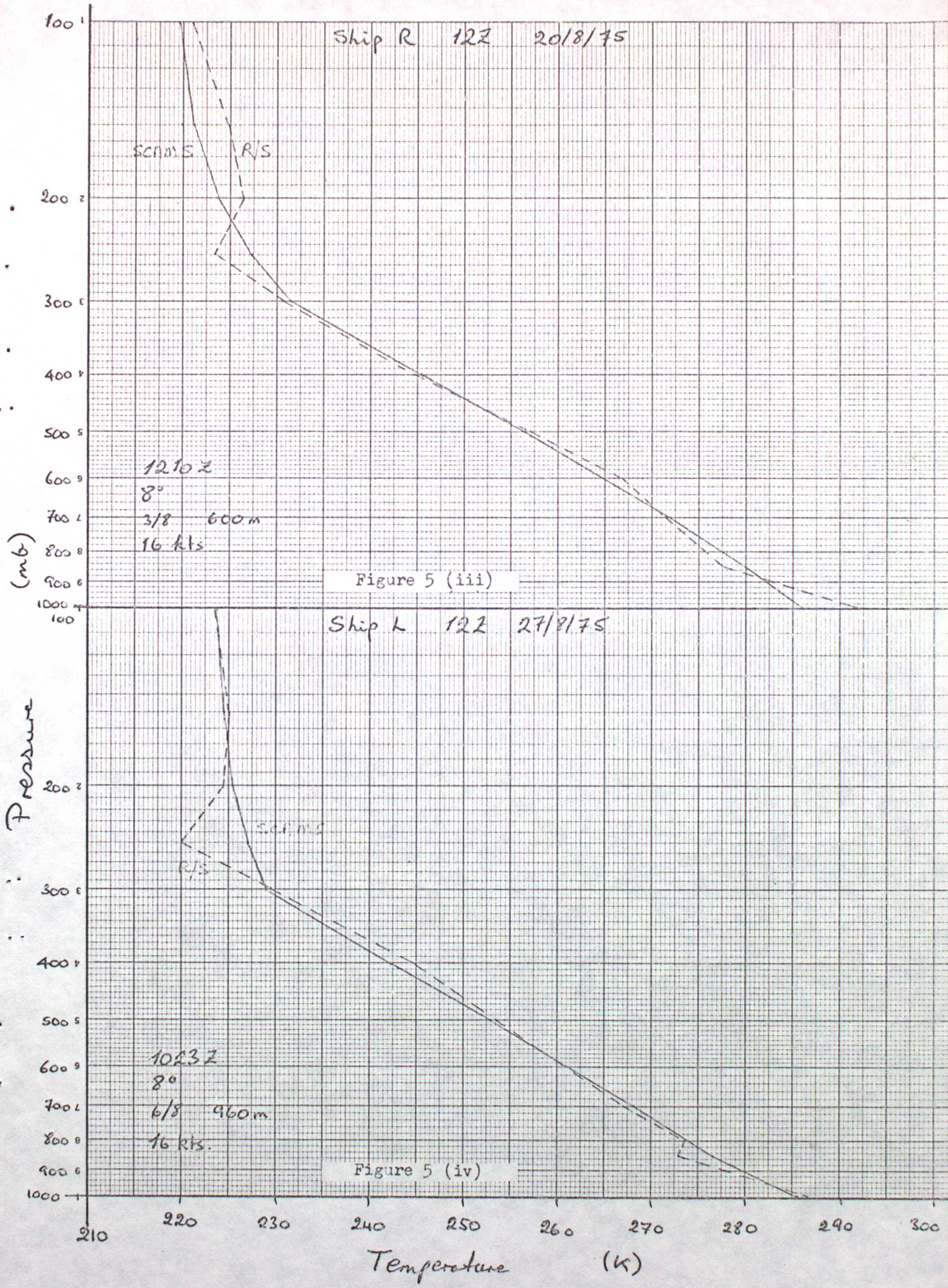
Ship R 12Z 20/8/75
SCANS
R/S
1210Z
8°
3/8 600m
16 kts
Figure 5 (iii)
Ship L 12Z 27/8/75
SCANS
R/S
1023Z
8°
6/8 960m
16 kts.
Figure 5 (iv)
Pressure (mb)
100
200
300
400
500
600
700
800
900
1000
210
220
230
240
250
260
270
280
290
300
Temperature (K)

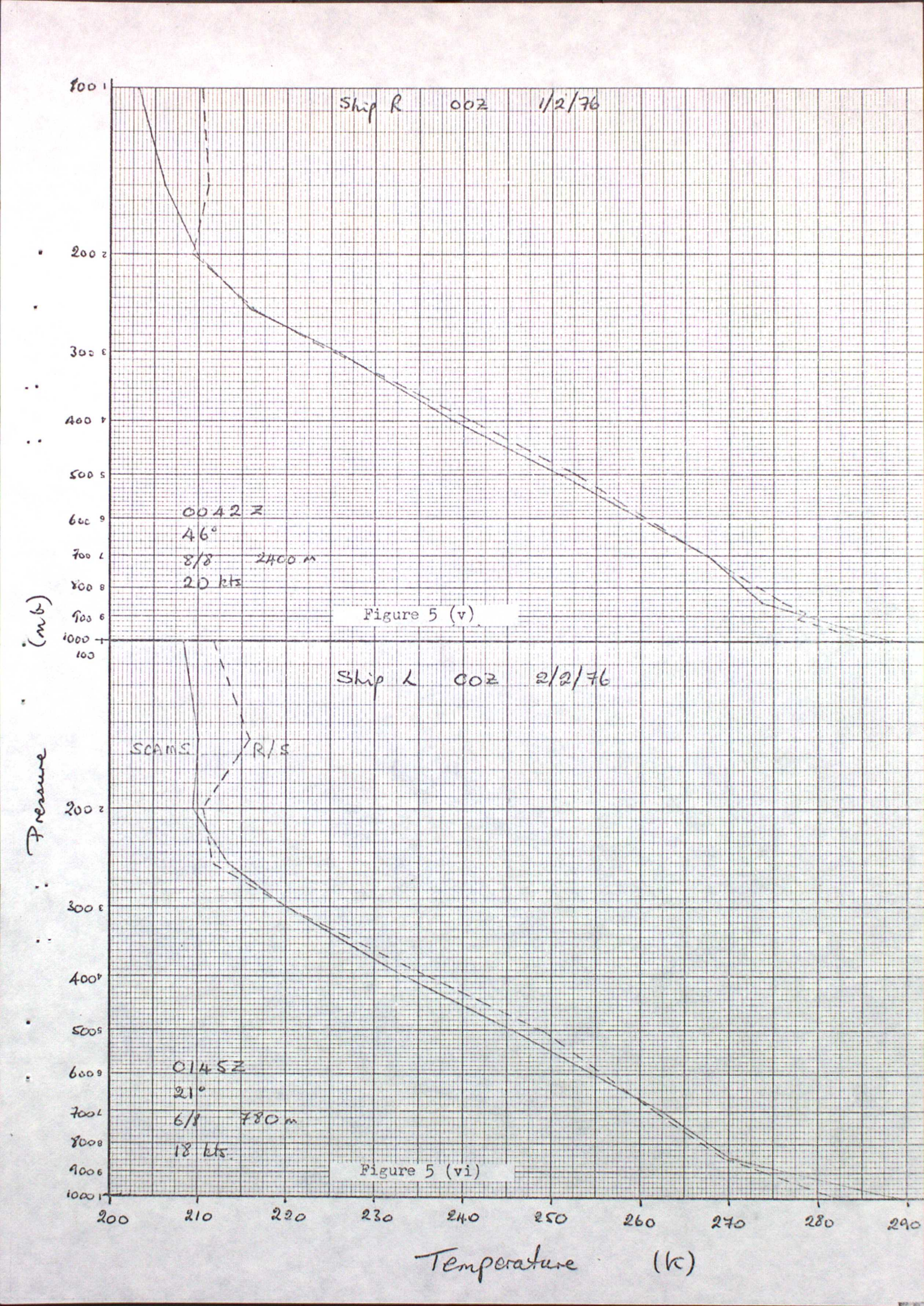
Ship R 00Z 1/2/76
0042 Z
46°
8/8 2400 m
20 kts
Figure 5 (v)
Ship L 00Z 2/2/76
SCAMS
R/S
0145Z
21°
6/8 780 m
18 kts
Figure 5 (vi)
Pressure (mb)
Temperature (K)
200
210
220
230
240
250
260
270
280
290

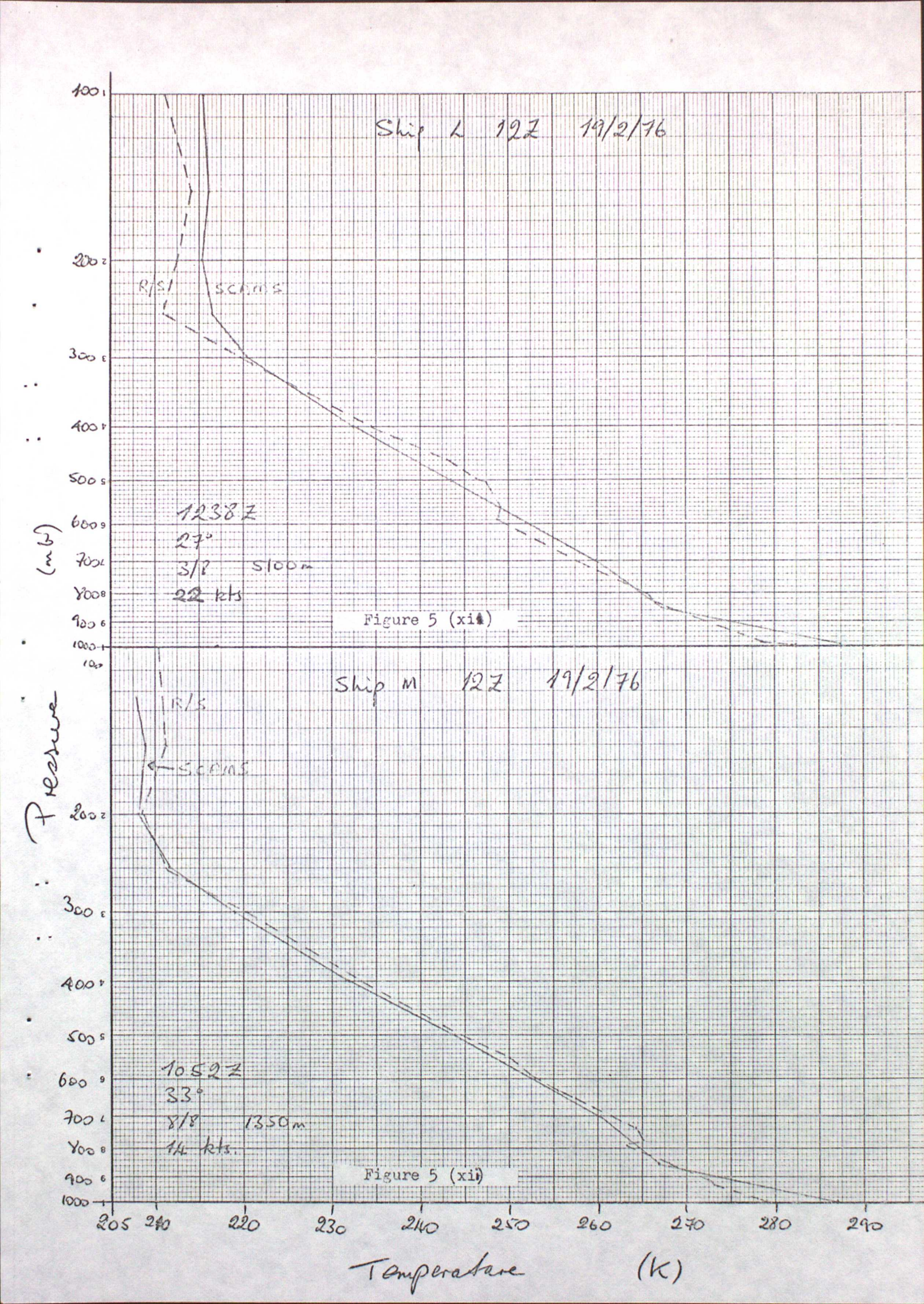
Ship L 12Z 19/2/76
R/S
SCANS
1238Z
27°
3/8 5100m
22 kts
Figure 5 (xi)
Ship M 12Z 19/2/76
R/S
SCANS
1052Z
33°
8/8 1350m
14 kts.
Figure 5 (xii)
Pressure (mb)
100
200
300
400
500
600
700
800
900
1000
205
210
220
230
240
250
260
270
280
290
Temperature (K)

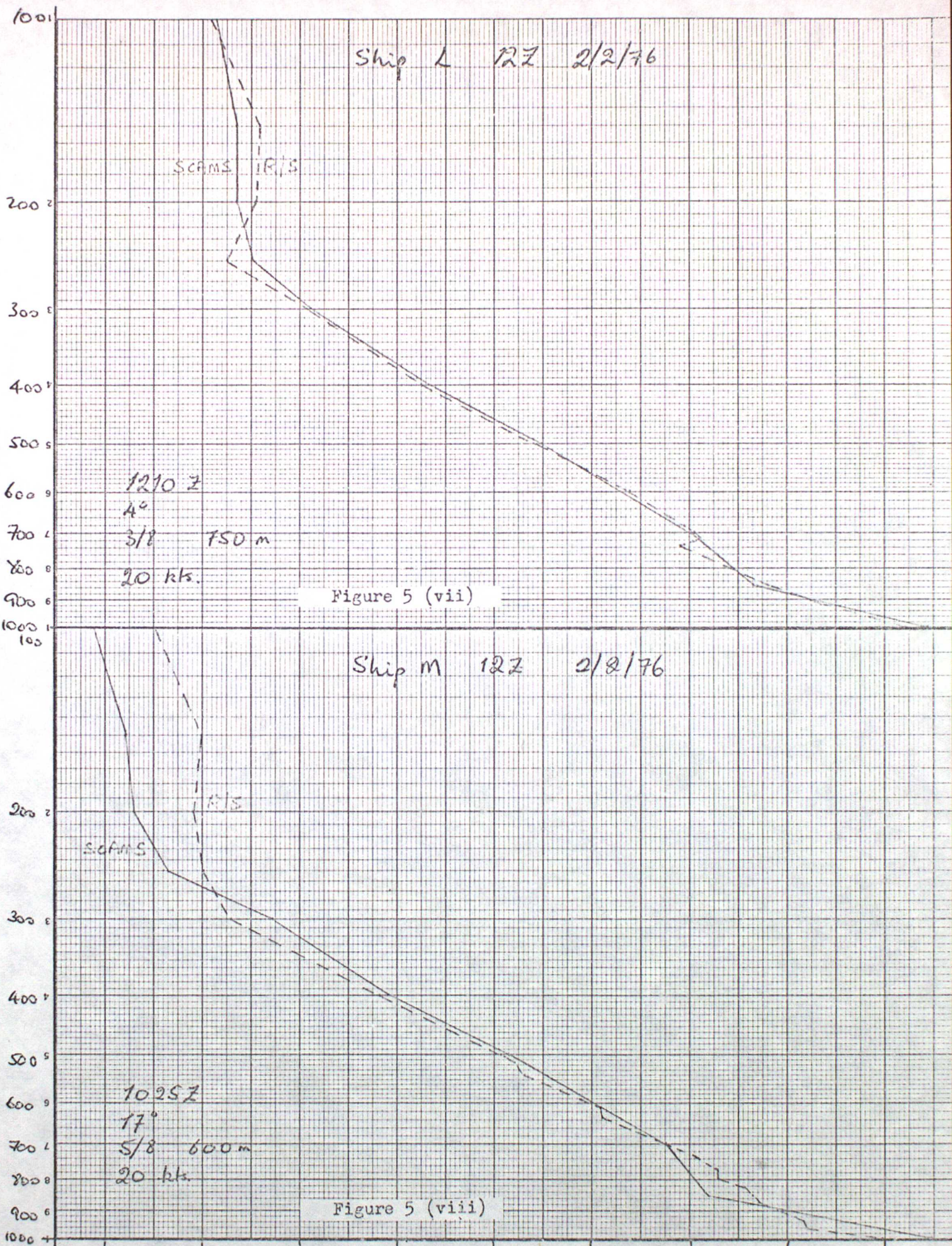

Figure 5 (vii)

Figure 5 (viii)

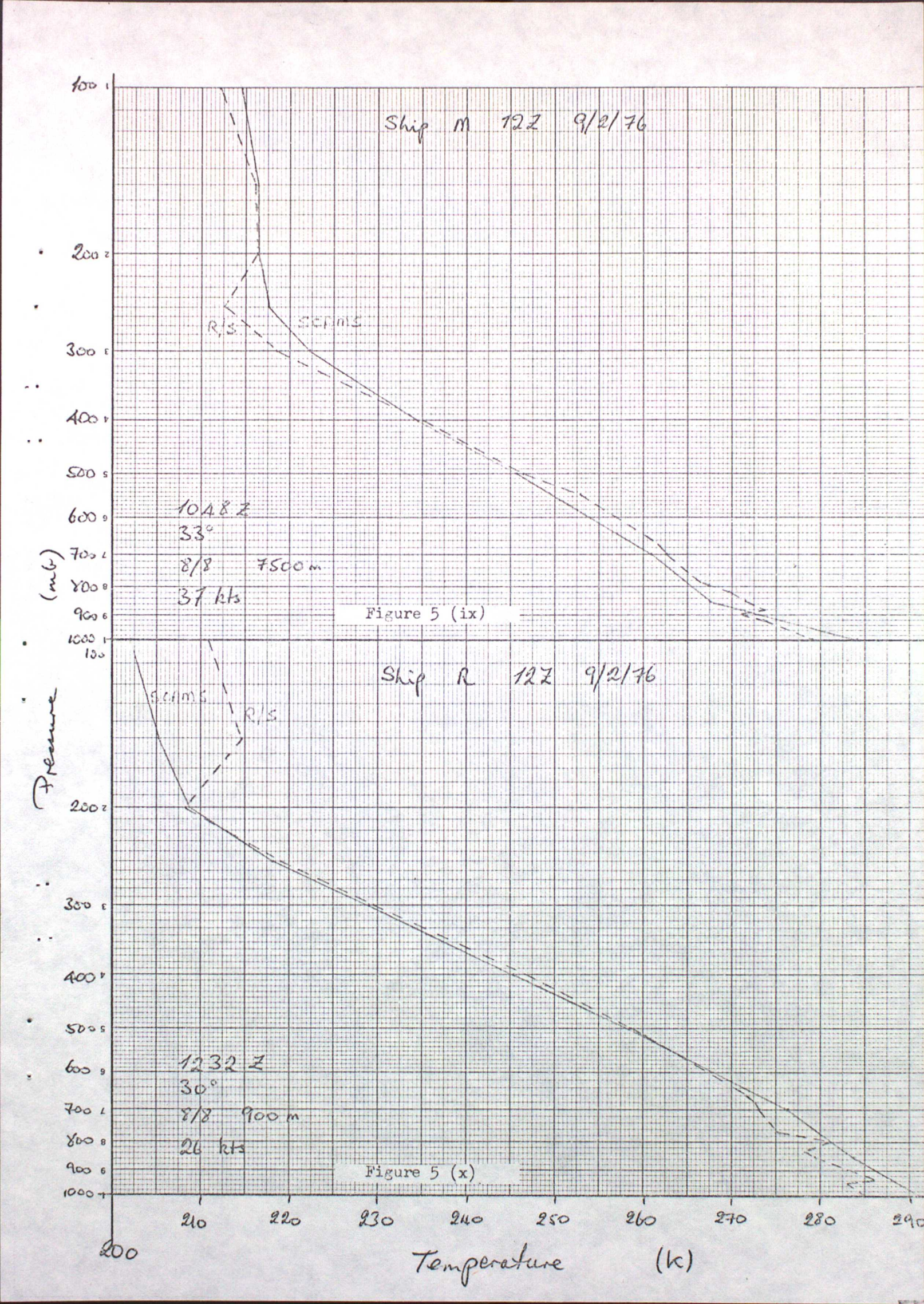
Ship M 12Z 9/2/76
R/S
SCIMS
1048 Z
33°
8/8 7500 m
37 kts
Figure 5 (ix)
Ship R 12Z 9/2/76
SCIMS
R/S
1232 Z
30°
8/8 900 m
26 kts
Figure 5 (x)
Pressure (mb)
Temperature (k)
100
200
300
400
500
600
700
800
900
1000
210
220
230
240
250
260
270
280
290
200

Figure 6. Independent sonde sample standard deviations and standard differences of (i) temperature and (ii) thickness.

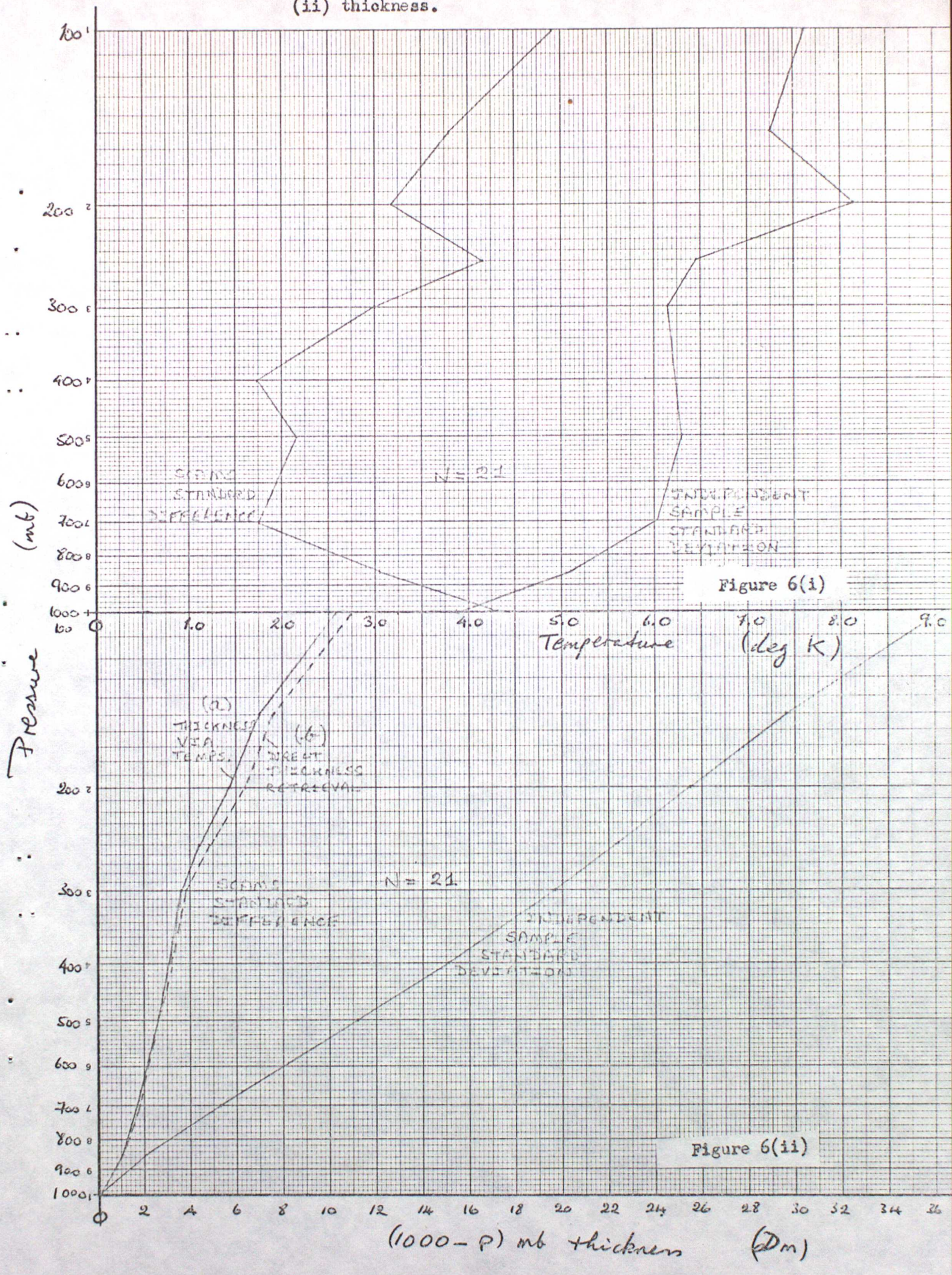

Figure 7. 1000-500 mb thickness fields from SCAMS retrievals (solid lines) and subjectively analysed CFO charts (dashed lines) for:

(i) 12Z 20 August 1975

(ii) 12Z 2 February 1976

(iii) 00Z 9 February 1976

(iv) 12Z 9 February 1976

(v) 00Z 14 February 1976

(vi) 00Z 19 February 1976

(vii) 12Z 19 February 1976.

The approximate times of each satellite pass are indicated along the bottom of the charts.


1000-500mb
THICKNESS
ANALYSED
SCAMS
RETRIEVED
1156Z
20/8/75
12Z
1009Z

Figure 7 (i)

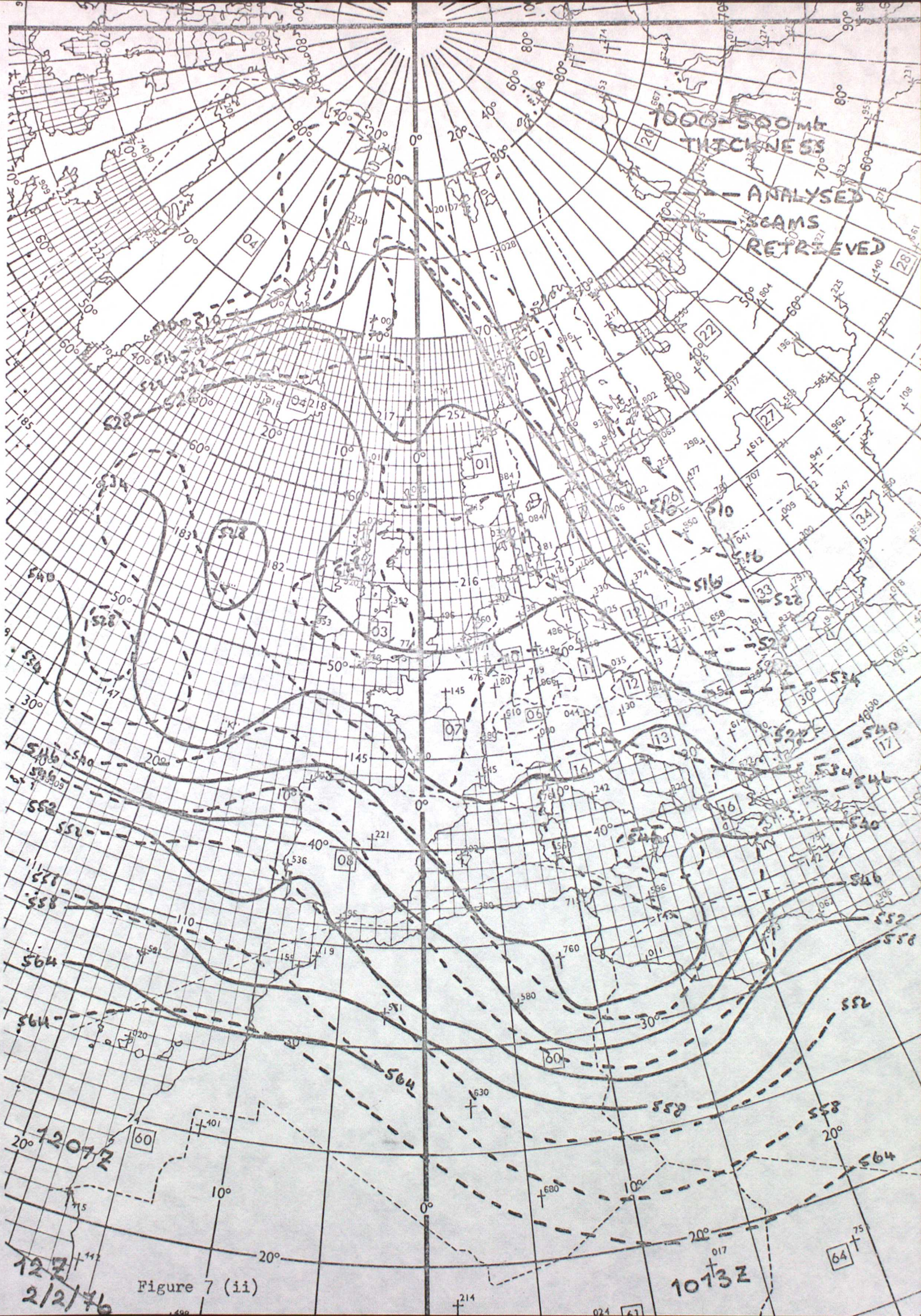
1000-500 mb
THICKNESS
ANALYSED
SCAMS
RETRIEVED
1207Z
1013Z
12Z
2/2/76

Figure 7 (ii)

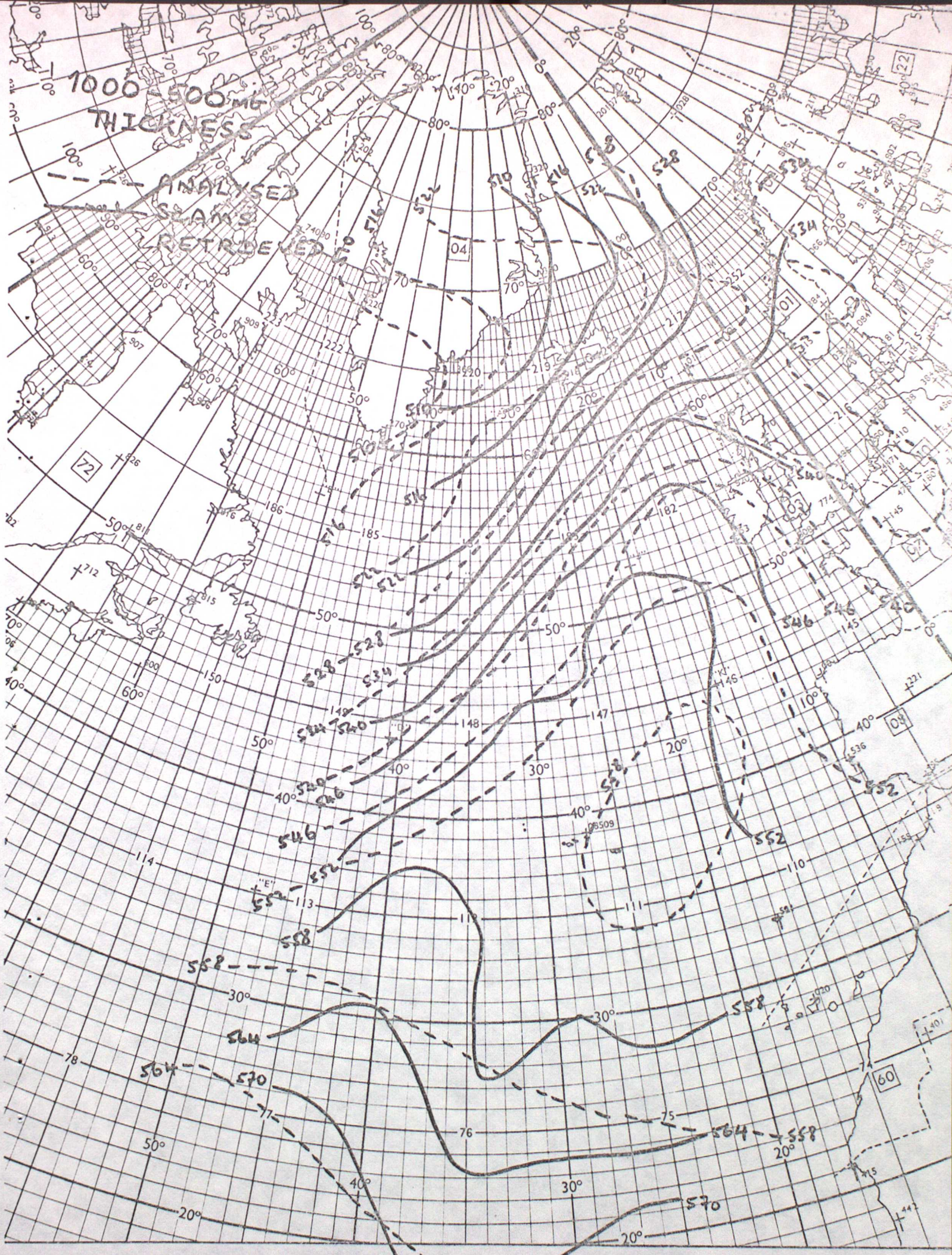

00Z
9/2/76

Figure 7 (iii)

0203Z.

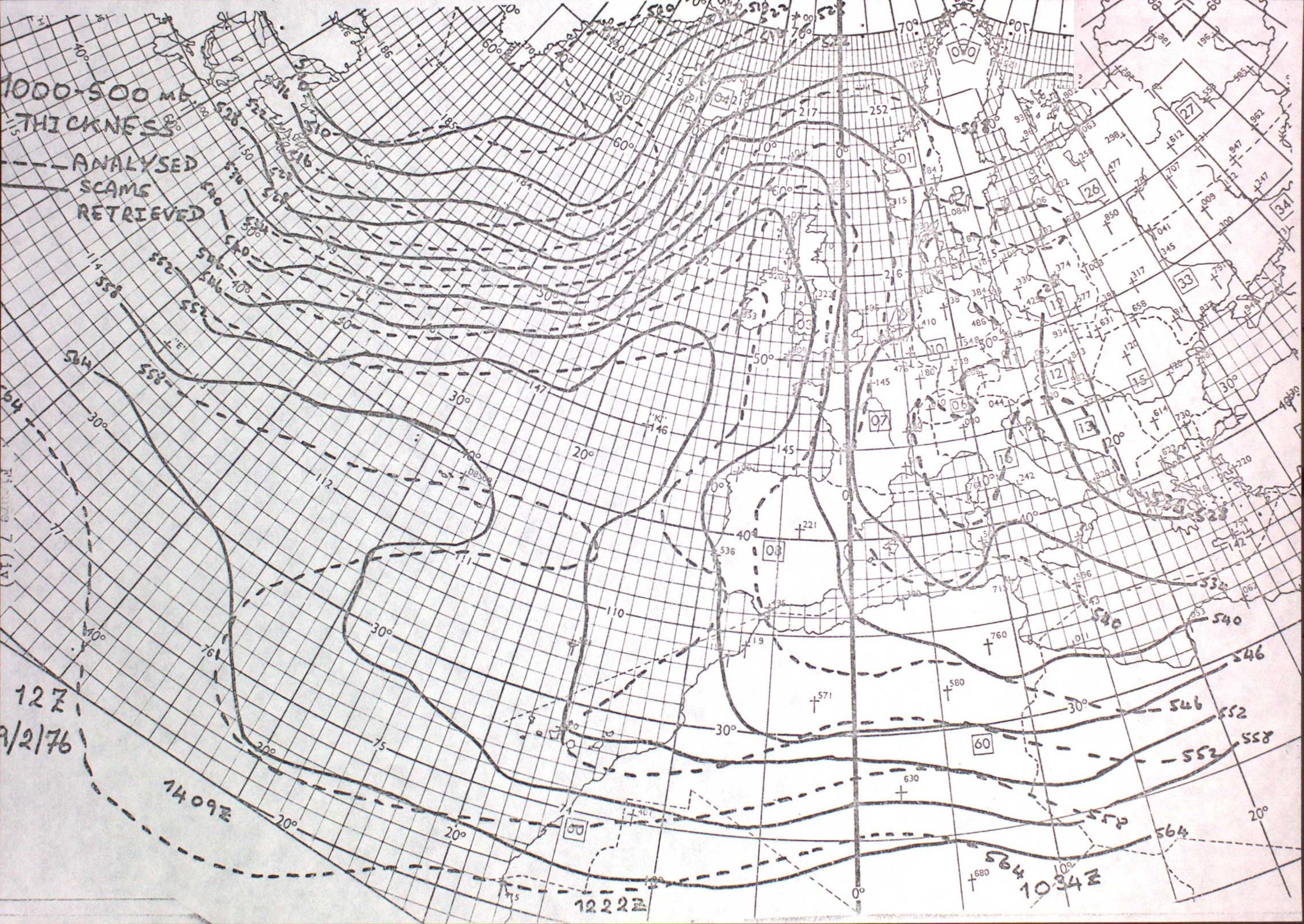
1000-500 MB
THICKNESS
ANALYSED
SCAMS
RETRIEVED
12Z
9/2/76
1409Z
1222Z
564
1034Z

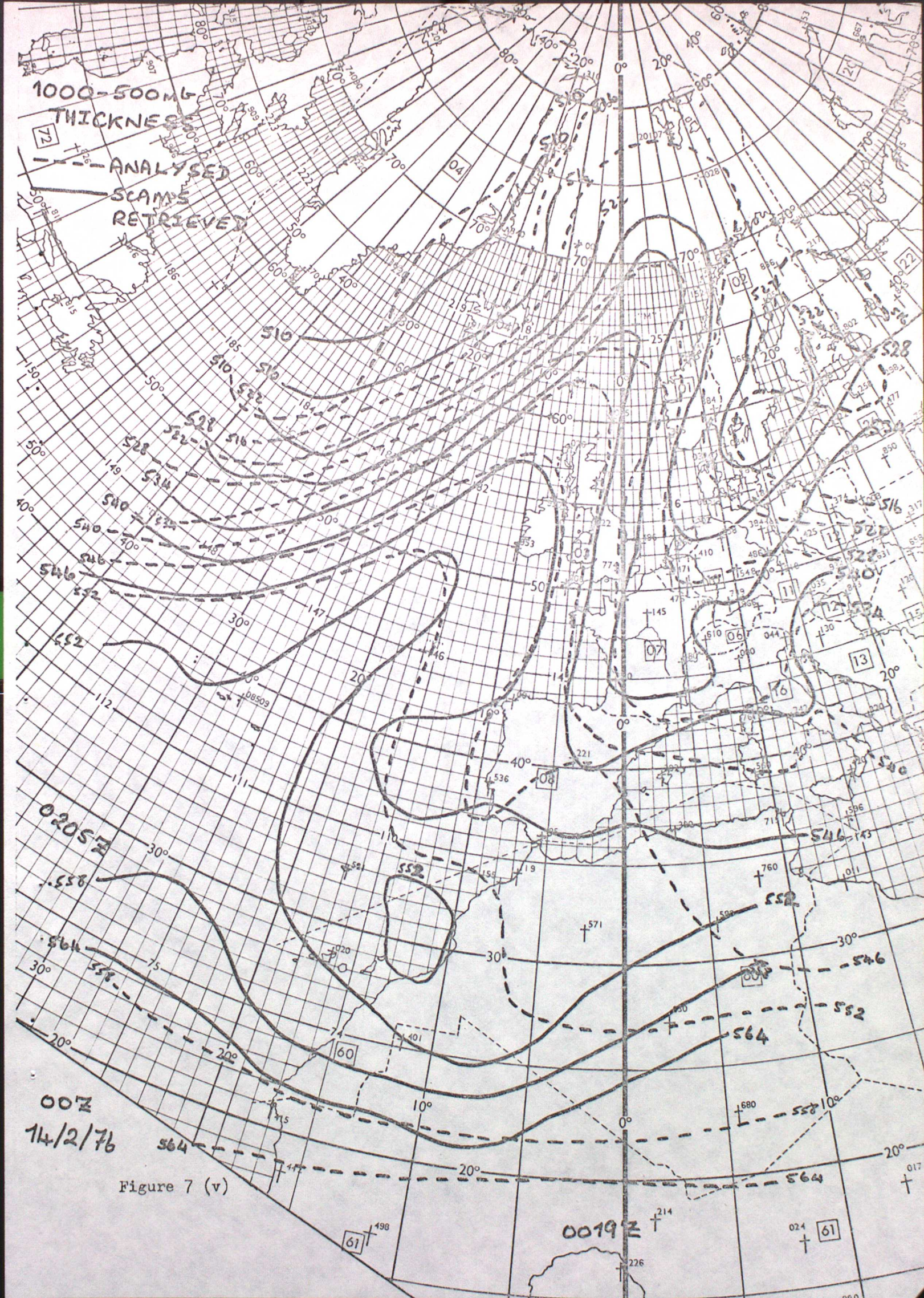
1000-500MB
THICKNESS
ANALYSED
SCAMS
RETRIEVED
0205Z
0019Z
00Z
14/2/76

Figure 7 (v)

Figure 7 (vi)

Figure 7 (vii)

FIGURE 8. A TYPICAL SCAMS RETRIEVAL PATTERN.

1000-500 MB THICKNESS VALUES (DM)

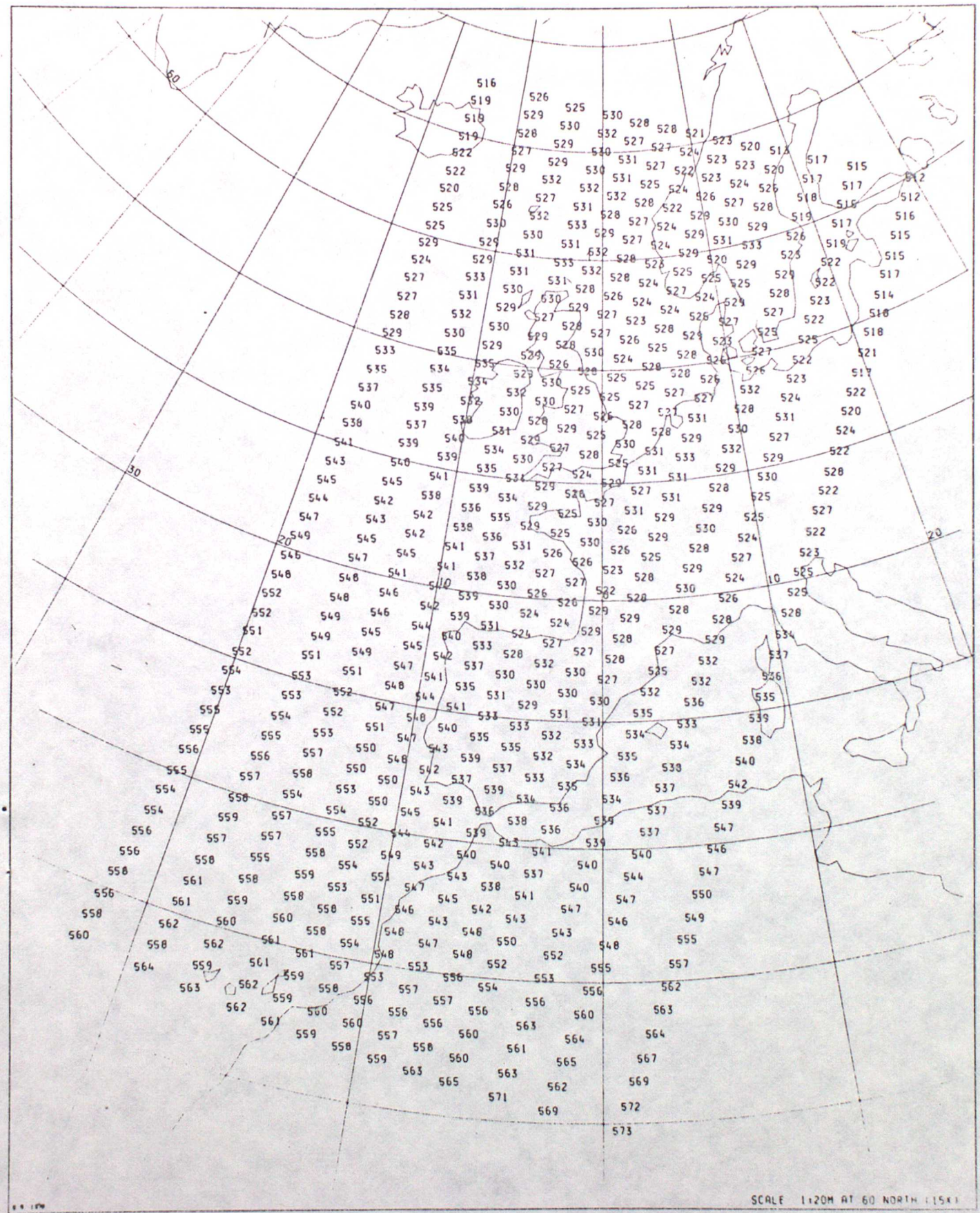

Appendix I: Surface Emissivity

In infrared work, the surface emissivity is usually taken to be 0.99 and independent of the nature of the surface. However, at microwave frequencies, the surface emissivity, ε_s , is very variable, being roughly 0.4-0.6 over sea and 0.9-1.0 over land. The value of ε_s depends on several factors: the polarisation of the emitted or reflected radiation; the zenith viewing angle; the frequency of the radiation. Additional factors over the sea are the salinity, temperature and wind speed (affecting roughness and foam generation). (Blume et al 1977, Gloersen and Barath, 1977, Ho and Hall, 1973, Rosenkranz and Staelin, 1972). Over land, the soil type and moisture content and vegitation type affect the emissivity.

At these microwave frequencies, especially over sea, the low surface emissivity causes not only a lowering of the apparent brightness temperature of the surface but also allows a significant amount of downward atmospheric emission to be reflected upward into a radiometer.

It is assumed that the surface emissivity (over sea) can be made up of a linear addition of emissivity contributions due to frequency (F), viewing angle (θ), temperature (T) and wind speed (W) (the small effects of salinity have been neglected).

ie

$$\varepsilon_p = \varepsilon_F + \varepsilon_\theta + \varepsilon_T + \varepsilon_w$$

P is H or V for horizontal or vertical polarisations.

where

$$\varepsilon_F = a_F + b_F . F$$

$$\varepsilon_\theta = (a_\theta + b_\theta . F) . \theta$$

$$\varepsilon_T = (a_T + b_T . F) . (T_s - 271) + (c_T + d_T . F)$$

$$\varepsilon_w = \left[(a_w + b_w . \theta) + F . (c_w + d_w . \theta)\right] . W$$

and the coefficients a and b depend on the ranges of the variables F, θ , T_s or W and on polarisation (horizontal or vertical). The values used in this study are a composite obtained from the above mentioned references, and are given in Tables API(i)-(iv).

The emissivity at intermediate polarisation is found by

$$\varepsilon_s(P) = \varepsilon_H + (\varepsilon_v - \varepsilon_H) \cdot \frac{P}{100}$$

where P is the percentage of vertical polarisation.

Appendix I References

Blume, H.C., A.W. Love, M.J. Van Melle, W.W. Ho, 1977:
Radiometric observations of sea temperature at 2.65 GHz over the Chesapeake Bay. IEEE Trans. Antennas Propagat., Vol AP-25, No 1, 121-128.

Gloersen, P, F.T. Barath, 1977: A scanning multichannel microwave radiometer for Nimbus-G and Seasat-A. IEEE J. Oceanic Eng., Vol OE-2, No 2, 172-178.

Ho, W, W.F. Hall, 1973: Measurements of the dielectric properties of seawater and NaCl solutions at 2.65 GHz. J. Geophys. Res., 78, No. 27, 6301-6315.

Rosenkranz, P.W., D.H. Staelin, 1972: Microwave emissivity of ocean foam and its effect on nadiral radiometric measurements. J. Geophys. Res. 77, No 33, 6528-6538.

Polarisation	a_F	b_F
H, V	0.359	5.2×10^{-3}

Table API(i). Emissivity coefficients for frequency in GHz.

Polarisation	a_θ	b_θ
H	2.5×10^{-3}	1.2×10^{-5}
V	-2.5×10^{-3}	-1.2×10^{-5}

Table API(ii). Emissivity coefficients for zenith angle in degrees.

Frequency (GHz)		a_w x 10^{-3}	b_w x 10^{-5}	c_w x 10^{-4}	d_w x 10^{-6}
F<10	H	2.10	4.11	1.22	- 1.95
	V	2.10	-4.11	1.22	1.95
F>10	H	3.21	1.19	0.12	0.95
	V	3.21	-1.19	0.12	-0.95

Table API (iii). Emissivity coefficients for wind speed in knots.

Surface Temp (K)		$a_T \times 10^{-4}$		$b_T \times 10^{-5}$		$c_T \times 10^{-3}$		$d_T \times 10^{-3}$	
		F<16	F>16	F<16	F>16	F<16	F>16	F<16	F>16
$T_s < 285$	H	6.7	- 1.9	- 13.5	- 7.9	0.0	0.0	0.0	0.0
	V	10.0	- 10.0	- 20.0	- 7.7	0.0	0.0	0.0	0.0
$T_s > 285$	H	6.1	6.1	- 7.1	- 7.1	1.5	- 16.1	- 1.1	0.0
	V	8.7	8.7	- 9.8	- 9.8	1.5	- 16.1	- 1.1	0.0

Table API (iv). Emissivity coefficients for surface temperature in kelvin.

Appendix II. Calculation of a Simulated Brightness Temperature

A model has been developed to calculate a simulated brightness temperature for a given set of conditions, based on equations (1), (2) and (3) in the main text. Profiles of height, pressure, temperature and humidity mixing ratio at discrete levels and microwave frequency are the primary inputs. From these quantities, the absorption coefficients per unit path length due to oxygen, α_o^i , (Rosenkranz, 1975) and water vapour, α_v^i , (Liebe, 1969) are calculated for each level i. If cloud is present, its base and total liquid water content are input; the cloud is assumed to be in a layer between the base level and the next higher level. The total absorption, α_c , through this depth of cloud is then calculated using the layer mean temperature (Staelin et al, 1976). The absorption coefficient due to any rain, α_R^i , is similarly found (Gloersen and Barath, 1977). This value is assumed to be a constant for i = ground to cloud base, zero at the cloud top and above.

Below the cloud base, the total absorption due to a layer is $\alpha^{i,i+1} = (\bar{\alpha}_o + \bar{\alpha}_v + \alpha_R).dh$ where dh is the thickness of the layer and $\bar{\alpha} = \frac{1}{2}(\alpha^i + \alpha^{i+1})$. The absorption within the cloud layer is $\alpha^{i = \text{cloud base}}_{\text{to cloud top}} = \alpha_c + (\bar{\alpha}_o + \bar{\alpha}_v + \frac{1}{2}\bar{\alpha}_R).dh$ and above the cloud is simply $\alpha^{i,i+1} = (\bar{\alpha}_o + \bar{\alpha}_v).dh$

The total transmission from level i (at height h^i) to the top of the profile is then

$$\tau^i = \exp\left\{-\sum_{j=i}^{N} \alpha^{j,j+1}\right\} \qquad \text{where } N = (\text{total no. of levels}) - 1$$

The weighting function at that level is, at zenith viewing angle θ and surface emissivity ε_s :

$$W^i = \left\{1 + (1-\varepsilon_s).\left[\frac{\tau^1}{\tau^i}\right]^{2\sec\theta}\right\}.\left\{\frac{(\tau^{i+1})^{\sec\theta} - (\tau^i)^{\sec\theta}}{h^{i+1} - h^i}\right\}$$

The surface contribution to the brightness temperature is

$$T_{B_s} = \varepsilon_s . T_s . (\tau^1)^{\sec\theta}$$

and the atmospheric contribution is

$$T_{B_a} = \sum_{i=1}^{N} \frac{1}{2} (T^i . w^i + T^{i+1} . w^{i+1}) . (h^{i+1} - h^i)$$

The total brightness temperature is then

$$T_B = T_{Bs} + T_{Ba}.$$

Appendix II References

Gloersen, P., F.T. Barath, 1977: A scanning multichannel microwave radiometer for Nimbus-G and Seasat-A. IEEE J. Oceanic Eng., Vol OE-2, No 2, 172-178.

Liebe, H.J., 1969: Calculated tropospheric dispersion and absorption due to the 22-GHz water vapour line. IEEE Trans. Antennas Propagat., Vol AP-17, No 5, 621-627.

Rosenkranz, P.W., 1975: Shape of the 5mm oxygen band in the atmosphere. IEEE Trans. Antennas Propagat. Vol AP-23, No 4, 498-506.

Staelin, D.H., K.F. Kunzi, R.L. Pettyjohn, R.K.L. Poon, R.W. Wilcox, J.W. Waters, 1976: Remote sensing of atmospheric water vapour and liquid water with the Nimbus 5 microwave spectrometer. J. Appl. Met., 15, 1204-1214.

Appendix III: A Sample of atmospheric profiles

A set of four hundred radiosonde profiles over a two year period was used to simulate a corresponding set of brightness temperatures. These mid-latitude (30-60°N and S) profiles were each of height, temperature and humidity mixing ratio at thirty pressure levels from 1000 to 10 mb. Since the majority of these profiles were over land, with extremes of temperature in the lowest few levels, a modified set of profiles was used for the 'sea' case. With this set, the 1000 mb temperature (also assumed to be the surface temperature) was constrained to be within the range 275-300K, then the temperature and mixing ratios (keeping the same relative humidities) up to 850 mb were altered to be consistent and the heights of each level recalculated. (See Figure AP III(i)). In cases where the 'surface' temperature was already within the above range, no changes were made.

In order to incorporate the effects of cloud on the simulated brightness temperatures, a layer of liquid water was introduced into many of the profiles. The 'cloud' was assigned a base level (see below) at one of the pressure levels and the cloud top assumed to be at the next higher level. Two methods were used to find a cloud base: firstly, the relative humidity (RH) was calculated from level No 2 (950 mb) upwards. The cloud base level was taken to be the lowest level at which the RH exceeded 0.9. A liquid water density proportional to (RH - 0.9) g cm^{-3} was assumed. If there were no such level below 500 mb, a second method was used. This was to generate a random number with a distribution shown in Table AP III(i). This shows that about one quarter of all the profiles (roughly 100) are cloud-free, and for example 18% of the profiles not containing cloud by the criteria of the first method have a cloud base at level 3. For profiles having a cloud base assigned in this way, a liquid water density was generated linearly within the range 0.0-0.1 g cm^{-3}. The total liquid water content, Q, was taken to be the product of liquid density, thickness of the cloud layer and a term falling exponentially with the height of the cloud base (simulating a smaller

liquid content with height, an increasing proportion of water as ice etc). The mixing ratios at the bottom and top of the cloud layer were then set equal to the saturated values. For each profile, an arbitrary value for wind speed was also generated for use in determining a surface emissivity (Appendix I).

Cloud base level	0	1	2	3	4	5	>5
Pressure level (mb)	NO CLOUD	1000	950	920	850	780	-
% of total	26	0	42	18	9	5	0

Table AP III(i). Percentage distribution of cloud base levels of profiles not containing cloud by a criterion of relative humidity.

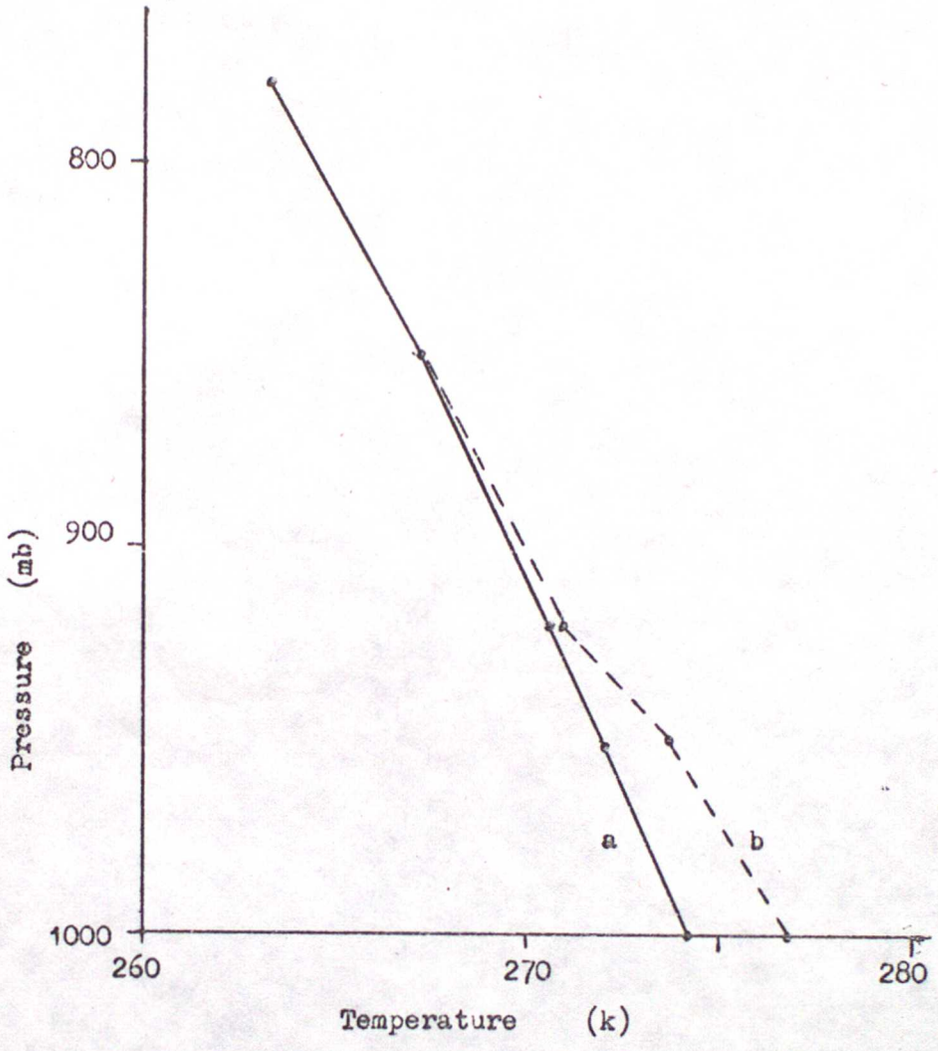

Figure AP III (i). An example of a radiosonde profile (curve (a)) modified for a sea surface (curve(b)).